Title	New iterative framework for frequency response mismatch correction in time-interleaved ADCs: Design and performance analysis
Author(s)	Tsui, KM; Chan, SC
Citation	IEEE Transactions on Instrumentation Aad Measurement, 2011, v. 60 n. 12, p. 3792-3805
Issued Date	2011
URL	http://hdl.handle.net/10722/155695
Rights	IEEE Transactions on Antennas and Propagation. Copyright © IEEE

New Iterative Framework for Frequency Response Mismatch Correction in Time-Interleaved ADCs: Design and Performance Analysis

K. M. Tsui and S. C. Chan, *Member, IEEE*

***Abstract*—This paper proposes a new iterative framework for the correction of frequency response mismatch in time-interleaved analog-to-digital converters. Based on a general time-varying linear system model for the mismatch, we treat the reconstruction problem as a linear inverse problem and establish a flexible iterative framework for practical implementation. It encumbrances a number of efficient iterative correction algorithms and simplifies their design, implementation, and performance analysis. In particular, an efficient Gauss–Seidel iteration is studied in detail to illustrate how the correction problem can be solved iteratively and how the proposed structure can be efficiently implemented using Farrow-based variable digital filters with few general-purpose multipliers. We also study important issues, such as the sufficient convergence condition and reconstructed signal spectrum, derive new lower bound of signal-to-distortion-and-noise ratio in order to ensure stable operation, and predict the performance of the proposed structure. Furthermore, we propose an extended iterative structure, which is able to cope with systems involving more than one type of mismatches. Finally, the theoretical results and the effectiveness of the proposed approach are validated by means of computer simulations.**

***Index Terms*—Farrow structures, frequency response mismatch, iterative methods, performance analysis, time-interleaved (TI) analog-to-digital converters (ADCs), variable digital filters (VDFs).**

I. Introduction

MODERN communication systems such as software-defined radios and other high-speed applications call for analog-to-digital converters (ADCs) with increasingly high sampling rate and low power consumption [1]. In general, the performance of an ADC is limited for a given process technology, e.g., IC fabrication [2]. In order to stay with the current technology while meeting the increasing requirements of modern communication systems, new structures for improving the performance of current signal converters are an important problem in both research and industrial communities. One promising approach that is capable of offering high sampling rate is time-interleaved (TI) ADCs [3], in which an array of ADCs works in parallel at a fraction of the overall sampling rate. If the outputs of the ADC array are combined appropriately, a much higher sampling rate than that of an individual ADC can be achieved. However, any small channel mismatches between sub-ADCs cause a significant degradation in performance [4], [5]. Therefore, correcting these mismatches in TI ADCs is of great importance. In particular, the correction of frequency response mismatches is the major concern of this paper.

A commonly encountered type of mismatch in TI ADCs is the time-skew errors between different channel ADCs, which has received great attention over the last decades. A number of solutions are now available [6]–[20], [39], [42]. In particular, the functionally weighted Lagrange interpolation in [16], the multichannel filter in [17], and the compensation structures in [18]–[20] are promising approaches for solving the timing mismatch problem. The former improves the conventional Lagrange interpolation [15] and offers good reconstruction accuracy, which increases with the interpolation order. However, when the timing mismatches change, the interpolation coefficients need to be recomputed online, which requires considerable number of general-purpose multipliers. Moreover, as the interpolation order increases, the window function for computing the interpolation coefficients exhibits very large value which makes fixed-point hardware implementation complicated. For high-speed applications, the large number of expensive general-purpose multipliers would increase significantly the hardware cost and power consumption [43]. The multichannel filter in [17] suffers from a similar online filter design problem, but it incorporates the prior knowledge of input spectrum to improve the accuracy, and the design complexity is low. On the other hand, the structures in [18]–[20] completely eliminate the need of expensive online filter design and, therefore, can be realized more efficiently with reduced implementation cost.

More recently, many research works have focused on the more general problem of frequency response mismatch, where the channel ADCs may have distinct magnitude and phase characteristics [21]–[25], [38], [41]. Among these works, the structure in [21] and a similar approach in [22] are particularly attractive for real-time applications because of the relatively lower reconfigurable complexity as in the timing mismatch compensation structures in [18]–[20]. In particular, the authors in [21] developed a system model for describing the general relationship between the input and output signals, analyzed the error signal due to frequency response mismatches, and demonstrated how the accuracy of the system can be progressively improved by cascading the compensation

Manuscript received November 18, 2010; revised March 3, 2011; accepted March 4, 2011. Date of publication May 2, 2011; date of current version November 9, 2011. This paper was presented in part at the *IEEE International Conference on Green Circuits and Systems 2010* [37]. The Associate Editor coordinating the review process for this paper was Dr. Rik Pintelon.

The authors are with the Department of Electrical and Electronic Engineering, The University of Hong Kong, Pokfulam, Hong Kong.

Digital Object Identifier 10.1109/TIM.2011.2141310

filters. An important advantage of this approach is that its implementation complexity is independent of the number of channels.

In this paper, we investigate the problem from another direction by considering it as an inverse problem of a time-varying linear system and propose a novel framework and structures for iterative correction of the frequency response mismatches in TI ADCs. In order to facilitate real-time implementation, we focus on the structure which works in a sample-by-sample manner. This can be viewed as an extension of the approach [19] for timing mismatch problem to the more complicated situation of frequency response mismatches. Furthermore, it will be shown that the compensation structure in [21], [22] actually corresponds to a classical iterative method, namely, Richardson iteration (RI), which is a special case of the proposed iterative framework. To further reduce the implementation complexity, we study in detail a more efficient iterative method based on Gauss–Seidel iteration (GSI), which, in general, has a convergence rate faster than that of the RI. Other methods such as successive overrelaxation (SOR) can also be used. Simulation results show that the GSI converges to the desired solution at a faster convergence rate than the RI. Since the GSI generally converges in two to three iterations, the structures of additional iterations can be cascaded for real-time applications.

Because of the time-varying nature of the frequency response mismatches, we propose to realize the compensation structure using variable digital filters (VDFs) [26]. Like the timing mismatch compensation in [18]–[20], the VDF can be designed to accommodate frequency response mismatches which are commonly described by a model with single spectral parameter. The resulting structure consists of a number of fixed coefficient subfilters and a few tuning parameters. Major advantages of the proposed structure are that the VDF coefficients involved can be varied online to cope with systems with gradually changing frequency characteristics, and more importantly, it can be implemented as the well-known Farrow structure with a limited number of variable multipliers, which are required to implement the tuning parameters [26], [27]. With the efficient finite wordlength hardware realization of the Farrow structure well-studied in [28], the overall reconstruction structure can be efficiently pipelined with only a few general multipliers for the tuning parameters.

Based on the proposed compensation structure, we also demonstrate how systems with timing and frequency mismatches can be compensated online. The basic idea is to compensate these mismatches successively using the proposed VDF-based structures. This is particularly useful when more than one type of mismatches, such as timing mismatch, frequency/bandwidth mismatch, etc., occur simultaneously.

Two important issues of the proposed iterative compensation structures are the condition for convergence and performance analysis. Such information will ensure their stable operation and help designers to predict their ultimate performances so as to select appropriate filter lengths and hardware resources to meet different design specifications. Owing to the rich theoretical analysis of iterative methods in mathematical communities [29], [40], we are able to derive useful results, such as sufficient conditions for convergence, and investigate the performance of the proposed iterative framework. Specifically, we derive expressions for the reconstructed signal spectrum and obtain a lower bound of signal-to-noise-and-distortion ratio (SNDR) by means of the classical bifrequency mapping for periodically time-varying digital filters first introduced in [30], [31]. The former is useful to quantify the performance of the proposed iterative structure by means of spurious free dynamic range (SFDR) and effective number of bits (ENOB). The latter helps to reveal how the SNDR is affected by the filter approximation error and convergence rate of the iterative methods. These results are useful to the performance prediction and evaluation of practical TI ADCs to be designed.

It should be noted that the proposed iterative framework extends significantly our previous work in [19], which solves the timing mismatch problem using the RI instead of the GSI. Moreover, a new representation of the proposed iterative framework is developed in joint time and frequency domain. It not only provides a general time-varying system model for better understanding of the proposed iterative framework but also facilitates the derivation of the important convergence and performance analyses. Apart from these important contributions, other issues such as the improved implementation structure and its extension to the case of multiple mismatches were also not considered in our previous work in [19]. In summary, these results and findings serve as a flexible framework for the development and analysis of other potentially more efficient iterative reconstruction algorithms such as the GSI considered in this paper.

This paper is organized as follows. Section II describes the problem of frequency response mismatches encountered in TI ADCs. The equivalent time-varying linear model and two particular examples of the proposed iterative structure, namely, the GSI and RI, for signal reconstruction, are then presented in Section III. Section IV is devoted to the realization of the approximated linear system model using VDFs. The efficient implementation of the GSI using the Farrow structure is also discussed. In Section V, the convergence and performance analyses of the proposed iterative structure are studied. Extension of the proposed VDF-based iterative structure to the more general cases of multiple time-varying mismatches, such as frequency response and timing mismatches, is discussed in Section VI. Design examples and comparisons with other conventional approaches are presented in Section VII. Finally, conclusion is drawn in Section VIII.

II. Background

In an M-channel TI ADC, M ADCs are operating in parallel, and the sampling instants between two adjacent ADCs differ by one system clock period. Ideally, if the M ADCs are functionally identical and the channel outputs are combined appropriately, we obtain an equivalent ADC having the same precision as the channel ADCs but offering a speed that is M times faster. However, any small mismatches between the M ADCs lead to degraded performance [4], [5].

Fig. 1 shows an M-channel TI ADC with frequency response mismatches, where $s_c(t)$ represents the input continuous-time

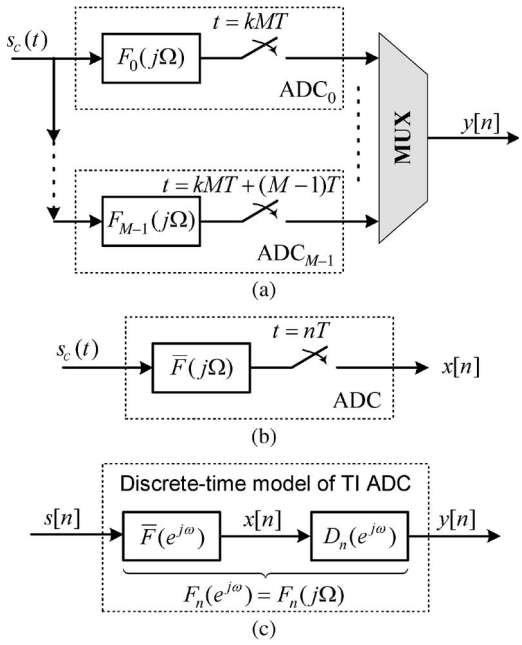

Fig. 1. (a) M-channel TI ADC with channel frequency response mismatches, (b) its equivalent circuit when all the channel responses are matched to $\overline{F}(j\Omega)$, and (c) its DT model.

(CT) signal and $F_n(j\Omega)$, for $n = 0, 1 \ldots, M-1$, represents the frequency responses of the channel analog filters. Because of the periodic sampling, $F_n(j\Omega)$ can also be treated as an M-periodic time-varying filter, i.e., $F_n(j\Omega) = F_{n+M}(j\Omega)$ for all n. The multiplexer selects one of the ADC outputs at a rate of $f_s = 1/T$ in a round-robin manner to form the output sequence $y[n]$. A typical example of channel frequency response is a phase shift in timing mismatch [6]–[20], where the sampling instants deviate slightly from the desired sampling grid due to clock skew or other imperfections. Most of these imperfections can be modeled as the channel frequency response $F_n(j\Omega)$. Usually, timing offset is estimated using, for example, the methods in [13], [14], [32], whereas the frequency response can be determined from circuit consideration with appropriate channel model [24].

Mismatches in the TI ADC occur when at least one channel frequency response is different from the others. Usually, it is advantageous to compensate for all channel frequency responses so that a desired time-invariant frequency response $\overline{F}(j\Omega)$ is obtained, i.e., $F_n(j\Omega) = \overline{F}(j\Omega)$ for $n = 0, 1 \ldots, M-1$[21]. This results in an equivalent single channel ADC shown in Fig. 1(b), where $s_c(t)$ is filtered by $\overline{F}(j\Omega)$ before sampling to obtain $x[n]$. As suggested in [21], such frequency distortion can be compensated, for example, via equalization in communication systems, which is commonly encountered in the single channel ADC. Therefore, the problem of correcting frequency response mismatches in TI ADC can be viewed as computing the desired $x[n]$ from the mismatched TI ADC output $y[n]$.

To this end, we shall first establish a discrete-time (DT) model for $x[n]$ and $y[n]$. Suppose that $s_c(t)$ is a band-limited CT signal with maximum frequency $f_{\max}$ and the sampling rate $f_s = 1/T$ is greater than the Nyquist rate $2f_{\max}$. Then, the equivalent DT relation of $s[n] = s_c(nT)$ and $y[n]$ in Fig. 1(a) can be expressed as

$$y[n] = \sum_{k=-\infty}^{\infty} s[k] \cdot f_n(n-k) \quad \forall n \tag{1}$$

where $f_n(n_0)$ is the DT impulse response of the time-varying channel filter $F_n(e^{j\omega}) = F_n(j\Omega)$, $|\omega| = |\Omega T| \leq \pi$. To establish the relation of $x[n]$ and $y[n]$, we further define the following M-periodic time-varying filter:

$$D_n(e^{j\omega}) = F_n(e^{j\omega})/\overline{F}(e^{j\omega}) \tag{2}$$

where $\overline{F}(e^{j\omega}) = \overline{F}(j\Omega)$, $|\omega| = |\Omega T| \leq \pi$, such that $F_n(e^{j\omega})$ can be viewed as a cascade of a time-invariant filter $\overline{F}(e^{j\omega})$ and a time-varying filter $D_n(e^{j\omega})$. Using (2), a DT model of TI ADC can be obtained, which depicts the relationship between $s[n]$, $x[n]$, and $y[n]$, as shown in Fig. 1(c). It can be seen that $x[n]$ is first obtained by filtering $s[n]$ via $\overline{F}(e^{j\omega})$ and is subsequently fed into $D_n(e^{j\omega})$ to produce $y[n]$. Hence, the input–output relationship of $x[n]$ and $y[n]$ is given by

$$y[n] = \sum_{k=-\infty}^{\infty} x[k] \cdot d_n(n-k) \quad \forall n \tag{3}$$

where $d_n(n_0)$ is the DT impulse response of $D_n(e^{j\omega})$. So far, we have described the ideal DT model of TI ADC with frequency response mismatches. Intuitively, we can see from (3) that $x[n]$ can be found by deconvoluting $y[n]$ with the known time-varying filter $d_n(n_0)$. Hence, the process of finding $x[n]$ given $d_n(n_0)$ is an inverse problem. However, such deconvolution is considerably complicated by the infinite support and time-varying nature of $d_n(n_0)$. To overcome this problem, we shall discuss hereinafter an efficient and practical approximation of $d_n(n_0)$, which forms an important part of the proposed iterative reconstruction method to be presented in Section III.

As in many previous works, we assume that $s_c(t)$ is slightly oversampled so that the DT Fourier transform (DTFT) of $s[n]$ is zero for $\alpha\pi \leq |\omega| \leq \pi$, $0 < \alpha < 1$. This slight reduction in operating bandwidth will generally lead to lower implementation complexity. By definition, the DTFT of $x[n]$ also satisfies this property. Consequently, the ideal filter $D_n(e^{j\omega})$ can be approximated by a filter with lower complexity, for example, finite length filter in the frequency band of interest (i.e., $0 \leq |\omega| \leq \alpha\pi$). Let $h_n[n_0]$ and $H_n(e^{j\omega})$ be the impulse and frequency responses of this filter. Then, (3) can be approximated as

$$y[n] \approx \sum_{k=n-N_{h2}}^{n+N_{h1}} x[k] \cdot h_n[n-k] \quad \forall n \tag{4}$$

where N_{h1} and N_{h2} are positive integers. When both N_{h1} and N_{h2} are finite, $h_n[n_0]$ can be realized as a finite-impulse response (FIR) filter. On the other hand, if N_{h1} and/or N_{h2} are infinite, $h_n[n_0]$ may alternatively be realized as an IIR filter. For simplicity, in the rest of this paper, we will mainly focus on the FIR case.

In practice, the differences between the two systems in (3) and (4) can be made arbitrarily small by reducing the approximation error between $D_n(e^{j\omega})$ and $H_n(e^{j\omega})$. Therefore, for notation convenience, we shall replace the approximate sign in (4) by the equality sign subsequently.

III. Versatile Iterative Framework

Consider the matrix form of (4) as follows:

$$\boldsymbol{y} = \boldsymbol{A}\boldsymbol{x} \tag{5}$$

where $\boldsymbol{y} = [y[-\infty], \ldots, y[\infty]]^{\mathrm{T}}$, $\boldsymbol{x} = [x[-\infty], \ldots, x[\infty]]^{\mathrm{T}}$, and $[\boldsymbol{A}]_{n,k} = a_{n,k} = h_n[n-k]$, $n, k = \ldots, -1, 0, 1, \ldots$. The problem at hand is to recover the uniform sequence $\boldsymbol{x}$, given its mismatched output $\boldsymbol{y}$. In other words, we want to solve the system of linear equations in (5). For the sake of presentation, $\{y[n]\}$ and $\{x[n]\}$ are assumed to be DT signals with finite and sufficiently large number of samples N for $n = 0, 1, \ldots, N-1$. Thus, $\boldsymbol{y}$ and $\boldsymbol{x}$ are now $(N \times 1)$ vectors, and $\boldsymbol{A}$ is a $(N \times N)$ matrix. Also, $h_n[n_0]$ is assumed to be noncausal. For practical implementation, it can be easily made causal by introducing appropriate delays.

For high-speed applications, directly inverting $\boldsymbol{A}$ to find $\boldsymbol{x}$ is undesirable due to excessive arithmetic complexity. In this paper, we propose to solve the inverse problem using iterative methods. For efficient implementation, we are interested in those which can be realized in a sample-by-sample manner. Most of them take the form of

$$\boldsymbol{B}\boldsymbol{x}^{(m+1)} = \boldsymbol{C}\boldsymbol{x}^{(m)} + \boldsymbol{y} \tag{6}$$

where $\boldsymbol{B} - \boldsymbol{C} = \boldsymbol{A}$ and $\boldsymbol{x}^{(m)}$ denotes the solution in the mth iteration.

The iterative framework in (6) is very flexible in the sense that we can choose different $\boldsymbol{B}$ and $\boldsymbol{C}$ for different iterative algorithms. For example, substituting $\boldsymbol{B} = \boldsymbol{I}$ and $\boldsymbol{C} = \boldsymbol{I} - \boldsymbol{A}$ into (6), one gets the RI as follows:

$$\boldsymbol{x}^{(m+1)} = (\boldsymbol{I} - \boldsymbol{A})\boldsymbol{x}^{(m)} + \boldsymbol{y}. \tag{7}$$

After a careful examination, it is noticed that the compensation structures in [21] and [22] actually belong to the RI. On the other hand, other iterative methods such as Jacobi iteration, GSI iteration, and SOR can also be used to achieve different tradeoffs between implementation complexity and convergence rate. Thus, (6) provides a general framework for solving the reconstruction problem using iterative methods, which greatly extends the previous works in [21] and [22].

In this paper, we consider the following GSI because of its faster convergence rate over the RI:

$$\boldsymbol{x}^{(m+1)} = (\boldsymbol{D} - \boldsymbol{L})^{-1}\boldsymbol{U}\boldsymbol{x}^{(m)} + (\boldsymbol{D} - \boldsymbol{L})^{-1}\boldsymbol{y} \tag{8}$$

where $\boldsymbol{B} = \boldsymbol{D} - \boldsymbol{L}$, $\boldsymbol{C} = \boldsymbol{U}$, $\boldsymbol{D}$ is the diagonal of matrix $\boldsymbol{A}$, and $\boldsymbol{L}$ and $\boldsymbol{U}$ are the negatives of the strictly lower and upper triangular parts of matrix $\boldsymbol{A}$, respectively. The equivalent time domain representation of (11) can be written as

$$\begin{aligned} x^{(m+1)}[n] = & h_n^{-1}[0]\left(y[n] - \sum_{k=n-N_{h2}}^{n-1} x^{(m+1)}[k]\cdot h_n[n-k]\right. \\ & \left. - \sum_{k=n+1}^{n+N_{h1}} x^{(m)}[k]\cdot h_n[n-k]\right), \\ & n = 0, \ldots, N-1. \end{aligned} \tag{9}$$

It can be seen that, apart from the addition of $\{y[n]\}$, the new iterate $\{x^{(m+1)}[n]\}$ is obtained from the convolution of $\{h_n[n_0]\}$ with $\{x^{(m)}[n]\}$ and the past samples of $\{x^{(m+1)}[n]\}$.

Now, we want to represent the matrix form of (6) in joint time and frequency domain for better understanding of the proposed iterative framework. In the context of time-varying system, the generalized frequency response of $h_n[n_0]$ in (4) can be expressed as [33]

$$H_n(e^{j\omega}) = \sum_{n_0=-N_{h1}}^{N_{h2}} h_n[n_0]e^{-j\omega n_0}. \tag{10}$$

For the RI in (7), $H_n(e^{j\omega})$ is split as $B_n(e^{j\omega}) = 1 - H_n(e^{j\omega})$ and $C_n(e^{j\omega}) = 1$, whereas, for the GSI in (8), $H_n(e^{j\omega})$ is split as $B_n(e^{j\omega}) = \sum_{n_0 \geq 0} h_n[n_0]e^{-j\omega n_0}$ and $C_n(e^{j\omega}) = -\sum_{n_0<0} h_n[n_0]e^{-j\omega n_0}$. Since $B_n(e^{j\omega})$ and $C_n(e^{j\omega})$ can be treated as time-invariant filters at time instant n[34], the RI and GSI as well as any other iterative methods under the framework of (6) can be represented as

$$B_n(e^{j\omega})X_n^{(m+1)}(e^{j\omega}) = C_n(e^{j\omega})X_n^{(m)}(e^{j\omega}) + Y_n(e^{j\omega}) \tag{11a}$$

$$B_n(e^{j\omega}) - C_n(e^{j\omega}) = H_n(e^{j\omega}) \tag{11b}$$

where $X_n^{(m)}(e^{j\omega})$ and $Y_n(e^{j\omega})$ are, respectively, the time-varying frequency responses of $x^{(m)}[n]$ and $y[n]$ at time instant n. Analogous to conventional linear time-invariant system, (11a) can be rewritten as

$$X_n^{(m+1)}(e^{j\omega}) = G_n(e^{j\omega})X_n^{(m)}(e^{j\omega}) + U_n(e^{j\omega})Y_n(e^{j\omega}) \tag{12}$$

where $G_n(e^{j\omega}) = B_n^{-1}(e^{j\omega})C_n(e^{j\omega})$ and $U_n(e^{j\omega}) = B_n^{-1}(e^{j\omega})$. Fig. 2 shows the signal flow graph of the proposed iterative algorithm which consists of M-periodic time-varying filters $G_n(e^{j\omega})$ and $U_n(e^{j\omega})$.

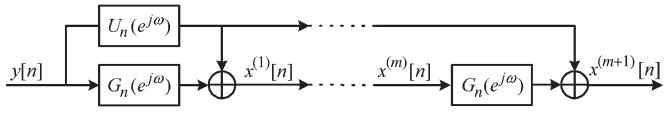

Fig. 2. General signal flow of the proposed iterative structure.

IV. Implementation Using VDF

In this section, we will illustrate how $\{h_n[n_0]\}$ in (9) can be implemented as VDFs so that the reconstruction problem can be realized as a process of digital filtering. The time-varying nature

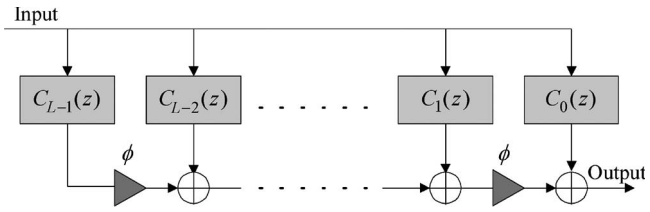

Fig. 3. Farrow structure for implementing a VDF.

of $h_n[n_0]$ naturally prompts us to consider the use of VDFs, which are able to vary their characteristics online by adjusting a tuning or spectral parameter ϕ. The basic idea to realize $h_n[n_0]$ using the VDF is to represent its impulse response as a polynomial in ϕ

$$h_n[n_0] = h[n_0,\phi]|_{\phi=\phi_n} = \sum_{l=0}^{L-1} c_l[n_0]\cdot\phi^l\Big|_{\phi=\phi_n} \tag{13}$$

where $h[n_0,\phi]$ is the impulse response of the VDF under consideration, in which the spectral parameter ϕ can be adjusted to ϕ_n to realize the time-varying nature of $h_n[n_0]$, L is the number of subfilters, and $c_l[n_0]$ is the impulse response of the lth subfilter. Here, we assume that $h_n[n_0]$ contains one type of time-varying mismatch which is characterized by the parameter ϕ in (13). The extension to the case of multiple time-varying mismatches will be discussed in Section VI. Furthermore, the z transform of the VDF can be expressed as

$$H(z,\phi)=\sum_{l=0}^{L-1} C_l(z)\phi^l=\sum_{l=0}^{L-1}\left[\sum_{n_0=-N_{h1}}^{N_{h2}} c_l[n_0]z^{-n}\right]\phi^l \tag{14}$$

where $C_l(z)$ is the z transform of the lth subfilters. Hence, the time-varying frequency response in (10) and that of the VDF in (14) are related by $H_n(e^{j\omega}) = H(e^{j\omega},\phi_n)$. Also, (14) suggests a famous Farrow structure for implementation as shown in Fig. 3. It can be seen that the Farrow structure consists of digital subfilters with fixed coefficients and a limited number of multipliers to implement the tuning parameter ϕ. Its efficient hardware implementation has been addressed in several related applications [20], [28].

We now consider the efficient implementation of the GSI using the Farrow structure mentioned earlier. First of all, with (13), we rewrite (9) as

$$x^{(m+1)}[n] = h^{-1}[0,\phi_n]\left(y[n]-s_1^{(m)}[n]-s_2^{(m)}[n]\right) \tag{15}$$

where $s_1^{(m)}[n]=\sum_{k=n-N_{h2}}^{n-1} x^{(m+1)}[k]\cdot h[n-k,\phi_n]$ and $s_2^{(m)}[n]=\sum_{k=n+1}^{n+N_{h1}} x^{(m)}[k]\cdot h[n-k,\phi_n]$. It is seen that $s_1^{(m)}[n]$ can be obtained by feeding $x^{(m+1)}[n]$ into a VDF $V_1(z,\phi)=\sum_{l=0}^{L-1} V_{1,l}(z)\cdot\phi^l$ with appropriate values of ϕ_n, where $V_{1,l}(z)=\sum_{n_0=1}^{N_{h2}} c_l[n_0]z^{-n}$ is the lth subfilter of $V_1(z,\phi)$. As for $s_2^{(m)}[n]$, the corresponding VDF is given by $V_2(z,\phi)=\sum_{l=0}^{L-1} V_{2,l}(z)\cdot\phi^l$, where $V_{2,l}(z)=\sum_{n_0=-N_{h1}}^{-1} c_l[n_0]z^{-n}$. Fig. 4(a) shows the resulting

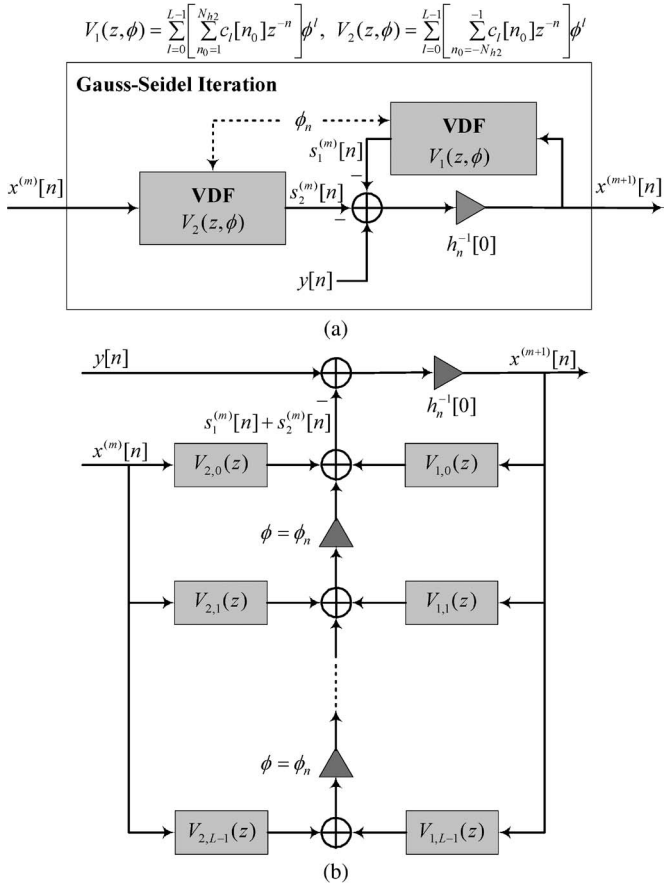

Fig. 4. (a) VDF-based correctors in the mth GSI. (b) Equivalent implementation structure with reduced number of tuning parameters.

TABLE I
IMPLEMENTATION COMPLEXITIES OF THE RI AND GSI IN ONE ITERATION. SUBFILTER LENGTH: $P = N_{h1} + N_{h2} + 1$; SUBFILTER NUMBER: L

	Number of non-trivial subfilter filter coefficients	ϕ_n	$h^{-1}[0,\phi_n]$
GSI	$L(N_{h1}+N_{h2})$	$L-1$	1
RI	LP	$L-1$	N/A

VDF-based structure for implementing the mth iteration of the GSI reconstruction algorithm. To further minimize the number of tuning parameters, the outputs of subfilters of $V_1(z,\phi)$ and $V_2(z,\phi)$ can be combined as shown in Fig. 4(b).

As mentioned earlier, the structures in [21] and [22] belong to the RI. In particular, we can see from the RI in (7) that $x^{(m)}[n]$ is fed into a VDF with transfer function $V_{RI}(z,\phi) = 1 - H(z,\phi)$. Therefore, the difference between RI and GSI is in the way of utilizing the VDF $H(z,\phi)$. Table I summarizes the implementation complexities of the RI and GSI in one iteration, where we assume that the subfilter length of the VDF is denoted by $P = N_{h1} + N_{h2} + 1$. We can see that the GSI has a complexity comparable to that of the RI. On the other hand, as will be demonstrated in Section VII, the GSI generally offers faster convergence rate than the RI, which leads to lower overall implementation complexity for pipelined operation.

V. Convergence and Performance Analyses

A. Sufficient Condition for Convergence

An important issue of iterative methods is the conditions for convergence. It is well known that the iteration in (6) converges for any $\boldsymbol{f}$ and $\boldsymbol{x}^{(0)}$ if and only if the spectral radius of $\boldsymbol{G} = \boldsymbol{B}^{-1}\boldsymbol{C}$ is less than one [29]. However, due to large value of N and time-varying coefficients $h_n[n_0]$ in $\boldsymbol{A}$, it is difficult to derive analytically a necessary and sufficient condition based on the spectral radius of $\boldsymbol{G}$. Therefore, we consider a simple sufficient condition which states that the iteration will converge for any $\boldsymbol{x}^{(0)}$ if and only if $\boldsymbol{A}$ is a strictly diagonal dominant matrix [29], [41]. That is, $|a_{n,n}| > \sum_{n\neq k}|a_{n,k}|$, for all n, which is equivalent to $|h_n[0]| > \sum_{n_0\neq 0}|h_n[n_0]|$, for all n. The latter condition can be tested numerically. Interested readers are referred to Appendix A for the proof of the sufficient condition for convergence of the GSI. Also, it is shown in Appendix B that the GSI should usually converge faster than the RI if $\boldsymbol{A}$ is a strictly diagonal dominant matrix. To test whether the diagonal of $\boldsymbol{A}$ is strictly dominant, we define

$$\lambda = \min_n \left\{ |h_n[0]| - \sum_{n_0\neq 0} |h_n[n_0]| \right\} \tag{16}$$

and check if λ is positive. This convergence condition can be readily checked, since $h_n[n_0] = h[n_0, \phi_n]$ in the form of VDF is known in practice after the design of the VDF $H(e^{j\omega}, \phi_n)$ to approximate $D_n(e^{j\omega})$.

It is remarked that the choice of $\overline{F}(e^{j\omega})$ plays an important role on the performance of iterative methods. A simple way is to choose $\overline{F}(e^{j\omega})$ such that $D_n(e^{j\omega}) = F_n(e^{j\omega})/\overline{F}(e^{j\omega})$ in (2) is close to one. This serves two main purposes. First, if $D_n(e^{j\omega})$ is well approximated by $H_n(e^{j\omega})$, then $\boldsymbol{A}$ becomes more diagonally dominant, and hence, the aforementioned convergence condition can be easily guaranteed. Second, the diagonal dominant matrix $\boldsymbol{A}$ will enhance the convergence rate of the iterative algorithm in (6) according to Appendix B. Therefore, the implementation complexity can be reduced with less number of iterations. This also agrees with the suggestion in [21], wherein $\overline{F}(e^{j\omega})$ is chosen as the average response of $F_n(e^{j\omega})$ through the analysis in frequency domain. However, it should be noted that the resulting spectrum after iterative correction would be close to $X(e^{j\omega}) = \overline{F}(e^{j\omega})S(e^{j\omega})$ instead of the original input spectrum $S(e^{j\omega})$ as illustrated in Fig. 1(b). Consequently, an additional compensation filter may be needed to compensate for $\overline{F}(e^{j\omega})$, if such frequency distortion cannot be tolerated. In this regard, one may alternatively choose $\overline{F}(e^{j\omega}) = 1$ to directly recover $S(e^{j\omega})$ in exchange for increased number of iterations and, hence, implementation complexity.

Another point worth mentioning is the effect of usable bandwidth on the implementation complexity of the proposed approach. If one wishes to reconstruct the signal spectrum very close to $\omega = \pi$, the condition number of the system matrix $\boldsymbol{A}$ deteriorates, and hence, more accurate approximation of the VDF and more iterations for reconstruction would be required. This, in turn, translates into higher implementation complexity, which is also an inherent problem of most other reconstruction algorithms. When the maximum sampling rate increases, the implementation complexity of the proposed approach only depends on the percentage of usable bandwidth (for example, longer filter length and more iterations will be needed) and is independent of the number of channels, although the data rate will be higher. Fortunately, since, unlike most other approaches, most of the multipliers in the proposed structure are fixed, the increase in the percentage of usable bandwidth would not introduce too much design and implementation burden particularly when the system changes due to variations in analog circuits.

Apart from the aforementioned convergence condition, it is also important to predict the ultimate performance and convergence rate of the general iterative algorithm in (6). In the following two sections, we shall analyze thoroughly the performance of the proposed iterative algorithm in joint time and frequency domain.

B. Spectrum of Reconstructed Signal and ADC Resolution

First of all, we denote $\hat{x}[n]$ as the solution of (5) upon convergence. In other words, $x^{(m)}[n]$ will approach $\hat{x}[n]$ as m increases, and thus, we have $y[n] = \sum_{k=n-N_{h2}}^{n+N_{h1}} \hat{x}[k]\cdot h_{\phi_n}[n-k]$ eventually. Similar to the relation between (6) and (11a), the time-varying frequency response of $y[n]$ at time instant n can be established as

$$Y_n(e^{j\omega}) = H_n(e^{j\omega})\hat{X}_n(e^{j\omega}) \tag{17}$$

where $Y_n(e^{j\omega})$, $H_n(e^{j\omega})$, and $\hat{X}_n(e^{j\omega})$ are all M-periodic time-varying frequency responses by definition. On the other hand, for the ideal TI ADC system model, (3) can also be written in joint time and frequency domain as

$$Y_n(e^{j\omega}) = D_n(e^{j\omega})X(e^{j\omega}). \tag{18}$$

From (17) and (18), we can see that if the approximation error between $H_n(e^{j\omega})$ and $D_n(e^{j\omega})$ is small, then $\hat{X}_n(e^{j\omega})$ will be close to $X(e^{j\omega})$.

As mentioned earlier, the iteration should converge for any initial guess once the sufficient condition is satisfied. Therefore, as in practical implementation, we select $x^{(0)}[n] = y[n]$ and hence

$$X_n^{(0)}(e^{j\omega}) = Y_n(e^{j\omega}). \tag{19}$$

By substituting this in the recursion in (12), we obtain

$$X_n^{(m+1)}(e^{j\omega}) = \left[G_n^{m+1}(e^{j\omega}) + \sum_{k=m}^{0} G_n^k(e^{j\omega})U_n(e^{j\omega}) \right] Y_n(e^{j\omega}) \tag{20}$$

where $G_n^k(e^{j\omega})$ denotes the kth power of $G_n(e^{j\omega})$. Further substituting (18) into (20), one gets

$$X_n^{(m+1)}(e^{j\omega}) = \Lambda_n^{(m+1)}(e^{j\omega})X(e^{j\omega}) \tag{21}$$

where $\Lambda_n^{(m+1)}(e^{j\omega}) = [G_n^{m+1}(e^{j\omega}) + \sum_{k=m}^{0} G_n^k(e^{j\omega})U_n(e^{j\omega})]D_n(e^{j\omega})$. We note that $X_n^{(m+1)}(e^{j\omega})$

can be considered as the output of the periodically time-varying system $\Lambda_n^{(m+1)}(e^{j\omega})$ with $X(e^{j\omega})$ as its input. Using the concept of bifrequency mapping in [30] and after some manipulations, the output spectrum of $x^{(m+1)}[n]$ can be expressed as

$$X^{(m+1)}(e^{j\omega}) = \sum_{k=0}^{M-1} \Gamma_k^{(m+1)}\left(e^{j\omega}W_M^k\right) X\left(e^{j\omega}W_M^k\right) \quad (22)$$

where $W_M = e^{-j2\pi/M}$ and $\Lambda_n^{(m+1)}(e^{j\omega})$ and $\Gamma_k^{(m+1)}(e^{j\omega})$ are related by the following discrete Fourier transform pair owing to the periodicity of $\Lambda_n^{(m+1)}(e^{j\omega})$ (i.e., $\Lambda_n^{(m+1)}(e^{j\omega}) = \Lambda_{n+M}^{(m+1)}(e^{j\omega})$):

$$\begin{cases} \Lambda_n^{(m+1)}(e^{j\omega}) = \sum\limits_{k=0}^{M-1} \Gamma_k^{(m+1)}(e^{j\omega}) W_M^{-nk} \\ \Gamma_k^{(m+1)}(e^{j\omega}) = \frac{1}{M} \sum\limits_{n=0}^{M-1} \Lambda_n^{(m+1)}(e^{j\omega}) W_M^{nk}. \end{cases} \quad (23)$$

Similar to perfect reconstruction filter banks [34], $\Gamma_0^{(m+1)}(e^{j\omega})$ should be close to one so as to retain the input spectrum $X(e^{j\omega})$, while $\Gamma_k^{(m+1)}(e^{j\omega})$, $k = 1, 2 \ldots, M-1$, should be close to zero so as to attenuate the aliasing components. As mentioned in Section II, owing to the approximation error between $H_n(e^{j\omega})$ and $D_n(e^{j\omega})$ in practice, perfect reconstruction can only be achieved approximately in the frequency band of interest.

As discussed in [2], an effective measure to quantify the performance of ADCs is the SFDR, which is the ratio of the single-tone signal amplitude to the largest nonsignal component within the spectrum of interest. Using (22) and (23), the worst-case SFDR after $(m+1)$ iterations is given by

$$SFDR_{\text{dB}}^{(m+1)} = \min_{\omega,k} 20\log_{10}\left|\Gamma_0^{(m+1)}(e^{j\omega})/\Gamma_k^{(m+1)}(e^{j\omega})\right| \quad (24)$$

for $\omega \in [-\alpha\pi, \alpha\pi]$ and $k = 1, 2 \ldots, M-1$. The corresponding ENOB after $(m+1)$ iterations, denoted by $ENOB^{(m+1)}$, can be approximated as [2]

$$ENOB^{(m+1)} = SFDR_{\text{dB}}^{(m+1)}/6.02 \text{ bits}. \quad (25)$$

Next, we will investigate how the filter approximation error affects the reconstruction accuracy of the solution. It should be noted that a different performance analysis was introduced in [21], which focus only on the RI, whereas this paper is applicable to any iterative methods in the form of (6) and takes into account the effect of filter approximation error.

C. SNDR

In this section, we shall derive a lower bound of SNDR of the TI ADC after frequency response mismatch correction. It gives insightful interpretation on the ultimate performance and convergence rate of the proposed iterative algorithm. The SNDR after $(m+1)$ iterations is given by

$$SNDR^{(m+1)} = \frac{\|\boldsymbol{x}\|^2}{\left\|\boldsymbol{x} - \boldsymbol{x}^{(m+1)}\right\|^2} = \frac{\int_{-\pi}^{\pi}\left|X(e^{j\omega})\right|^2 d\omega}{\int_{-\pi}^{\pi}\left|X(e^{j\omega}) - X^{(m+1)}(e^{j\omega})\right|^2 d\omega} \quad (26)$$

where $\|\boldsymbol{x}\|$ denotes the Euclidean norm of $\boldsymbol{x}$. Note that we have used Parseval's theorem for periodically time-varying signal. The proof is not difficult, and interested readers are referred to [35] for more details. It is shown in Appendix C that the lower bound of SNDR after $(m+1)$ iterations is given by

$$SNDR^{(m+1)} \geq \frac{M}{\sum\limits_{n=0}^{M-1}\int_{-\alpha\pi}^{\alpha\pi}\left|P_n(e^{j\omega}) + G_n^{m+1}(e^{j\omega})Q_n(e^{j\omega})\right|^2 d\omega} \quad (27)$$

where $P_n(e^{j\omega}) = 1 - D_n(e^{j\omega})H_n^{-1}(e^{j\omega})$ and $Q_n(e^{j\omega}) = D_n(e^{j\omega})[H_n^{-1}(e^{j\omega}) - 1]$. We can see that $P_n(e^{j\omega})$ represents the filter approximation error between $H_n(e^{j\omega})$ and $D_n(e^{j\omega})$, which affects the SNDR due to the use of practical filter. Also, $G_n(e^{j\omega})$ is the only function that determines the characteristics of the iterative methods under the framework in (9). For example, $G_n(e^{j\omega}) = (-\sum_{n_0<0} h_n[k]e^{-j\omega n_0})/(\sum_{n_0\geq 0} h_n[k]e^{-j\omega n_0})$ for the GSI, whereas $G_n(e^{j\omega}) = 1 - H_n(e^{j\omega})$ for the RI. In fact, $G_n(e^{j\omega})$ indicates how fast the iteration converges. More precisely, the smaller it is, the faster convergence rate the iterative method can achieve. The requirement of small $G_n(e^{j\omega})$ also coincides with the sufficient condition considered in Section V-A.

Furthermore, if the iteration does converge, then we have

$$\lim_{m\to\infty} G_n^{m+1}(e^{j\omega}) = 0. \quad (28)$$

As a result, the ultimate SNDR for any iterative algorithms under the framework in (12) is eventually governed by $P_n(e^{j\omega})$, i.e., the approximation error between the designed and desired filter responses and its lower bound is given by

$$SNDR_{\text{ult}} \geq \frac{M}{\sum\limits_{n=0}^{M-1}\int_{-\alpha\pi}^{\alpha\pi}\left|P_n(e^{j\omega})\right|^2 d\omega}. \quad (29)$$

The aforementioned analysis provides valuable information for system designers to evaluate and estimate the achievable performance of the general iterative method in (6).

VI. Extension to Cascade of Multiple Time-Varying Systems

As mentioned earlier, various types of mismatches exist in TI ADCs, such as the commonly encountered timing mismatch, bandwidth mismatch, etc. Very often, more than one type of mismatch may occur simultaneously. Assuming that each of

them can be modeled as a linear time-varying system, the ideal system in (18) can be expressed as

$$Y_n(e^{j\omega}) = \prod_{i=1}^{I} D_{n,i}(e^{j\omega})X(e^{j\omega}) = D_n(e^{j\omega})X(e^{j\omega}) \quad (30)$$

where I is the number of the time-varying systems. If we directly apply the proposed iterative algorithm to find $X(e^{j\omega})$, the resulting VDF will become a multidimension function characterized by one frequency variable and I tuning parameters. Therefore, the reconstruction will become very complicated due to the high design and implementation complexities of high-dimension VDF for large I. In this section, we will propose an efficient structure based on our structure developed in Sections III and IV to deal with this scenario.

Following the approaches in Sections III and IV, we approximate each ideal time-varying systems $D_{n,i}(e^{j\omega})$ by a practical filter $H_{n,i}(e^{j\omega})$ for $i = 1, 2, \ldots, I$ in the frequency band of interest. The overall system can therefore be expressed in matrix form as

$$\boldsymbol{y} = \left(\prod_{i=1}^{I} \boldsymbol{A}_i\right)\boldsymbol{x} \quad (31)$$

where the nth row of $\boldsymbol{A}_i$ relates to the impulse response of $H_{n,i}(e^{j\omega})$, $h_{n,i}[n_0]$, as in (5). The system in (31) can be further partitioned as

$$\boldsymbol{w}_{i-1} = \boldsymbol{A}_i\boldsymbol{w}_i, \qquad i = 1, 2, \ldots, I \quad (32)$$

where we define $\boldsymbol{w}_0 = \boldsymbol{y}$ and $\boldsymbol{w}_I = \boldsymbol{x}$. Assuming that the system matrix $\boldsymbol{A}_i$ satisfies the sufficient condition for convergence, the proposed iterative algorithm in (6) can be employed to solve $\boldsymbol{w}_i$ by the following recursion:

$$\boldsymbol{B}_i\boldsymbol{w}_i^{(m_i+1)} = \boldsymbol{C}_i\boldsymbol{w}_i^{(m_i)} + \boldsymbol{w}_{i-1} \quad (33)$$

where $\boldsymbol{A}_i = \boldsymbol{B}_i - \boldsymbol{C}_i$. Its time-varying frequency response at time instant n is given by

$$W_{n,i}^{(m_i+1)}(e^{j\omega}) = G_{n,i}(e^{j\omega})W_{n,i}^{(m_i)}(e^{j\omega}) + U_{n,i}(e^{j\omega})W_{n,i-1}(e^{j\omega}) \quad (34)$$

where $G_{n,i}(e^{j\omega}) = B_{n,i}^{-1}(e^{j\omega})C_{n,i}(e^{j\omega})$, $U_{n,i}(e^{j\omega}) = B_{n,i}^{-1}(e^{j\omega})$, and $H_{n,i}(e^{j\omega}) = B_{n,i}(e^{j\omega}) - C_{n,i}(e^{j\omega})$. Suppose that K_i denotes the number of iterations used for the reconstruction of the ith time-varying system, the proposed approach starts with an initial guess $\boldsymbol{w}_1^{(0)} = \boldsymbol{y}$, and after K_1 iterations, $\boldsymbol{w}_1^{(K_1)}$ is obtained as the solution of the first system $\boldsymbol{y} = \boldsymbol{w}_0 = \boldsymbol{A}_1\boldsymbol{w}_1$. Then, $\boldsymbol{w}_1^{(K_1)}$ is used as the initial guess of the next system $\boldsymbol{w}_1^{(K_1)} = \boldsymbol{A}_2\boldsymbol{w}_2$. The process is repeated until the last system $\boldsymbol{w}_{I-1}^{(K_{I-1})} = \boldsymbol{A}_I\boldsymbol{w}_I$ is iteratively solved to find $\boldsymbol{w}_I^{(K_I)}$, which should be close to $\boldsymbol{x}$ if K_i, $i = 1, 2, \ldots, I$, is sufficiently large. Fig. 5 illustrates an example for $I = 2$, where the target system is formed by a cascade of two time-varying channel frequency responses and the corresponding reconstruction structure consists of two consecutive iterative algorithms.

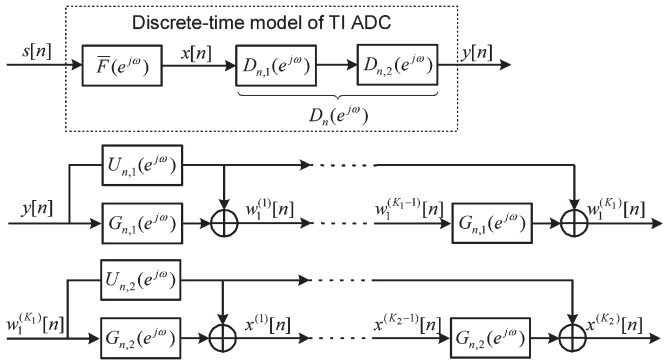

Fig. 5. (Upper figure) DT model of TI ADC with a cascade of two types of channel frequency responses, and (middle and lower figures) the general iterative reconstruction structures for the first and second systems.

Similar to the discussions in Section V, we can derive the output spectrum and the lower bound of SNDR for the aforementioned algorithm. Since the derivation of the former is straightforward, we only focus on the analysis of the SNDR performance due to page limitation. Without loss of generality, we consider the overall reconstruction structure shown in Fig. 5. First of all, we define $\hat{\boldsymbol{w}}_1$ and $\hat{\boldsymbol{x}}$, respectively, as the ultimate solutions of the systems $\boldsymbol{y} = \boldsymbol{A}_1\boldsymbol{w}_1$ and $\boldsymbol{w}_1^{(K_1)} = \boldsymbol{A}_2\boldsymbol{x}$ so that their time-varying frequency responses satisfy

$$Y_n(e^{j\omega}) = H_{n,1}(e^{j\omega})\hat{W}_{n,1}(e^{j\omega}) \quad (35)$$

$$W_{n,1}^{(K_1)}(e^{j\omega}) = H_{n,2}(e^{j\omega})\hat{X}_n(e^{j\omega}). \quad (36)$$

Moreover, according to the earlier discussions, the initial guess to the second system is

$$X_n^{(0)}(e^{j\omega}) = W_{n,1}^{(K_1)}(e^{j\omega}). \quad (37)$$

Similar to (A10) in Appendix C, $W_{n,1}^{(K_1)}(e^{j\omega})$ can also be expressed as

$$W_{n,1}^{(K_1)} = \hat{W}_{n,1} - G_{n,1}^{K_1}(\hat{W}_{n,1} - Y_n). \quad (38)$$

Note that, for notation simplicity, we have dropped the frequency argument $(e^{j\omega})$. From (38), we can see that $W_{n,1}^{(K_1)}$ approaches the ultimate solution $\hat{W}_{n,1}$ if $G_{n,1}$ is small and $G_{n,1}^{K_1}$ becomes negligible for sufficiently large K_1. Otherwise, such residue will propagate to the second system, as we shall consider in the following. Using (30) and (35)–(38) and after some manipulations, (A8) in Appendix C can be written as

$$R_n^{(K_1,K_2)} = [X - \hat{X}_n] + G_{n,2}^{K_2}\left[\hat{X}_n - X_n^{(0)}\right] = \left[P_n + G_{n,1}^{K_1}Q_{n,1} + G_{n,2}^{K_2}Q_{n,2}\right]X \quad (39)$$

where $P_n = 1 - D_nH_{n,1}^{-1}H_{n,2}^{-1}$, $Q_{n,1} = (H_{n,1}^{-1} - 1)H_{n,2}^{-1}D_n$, and $Q_{n,2} = (1 - H_{n,2})(1 - P_n - G_{n,1}^{K_1}Q_{n,1})$. To highlight the difference with (A8) in Appendix C, the superscript (K_1, K_2) is used here to represent that $R_n^{(K_1,K_2)}$ is obtained by applying K_1 iterations to the first system, followed by K_2 iterations to

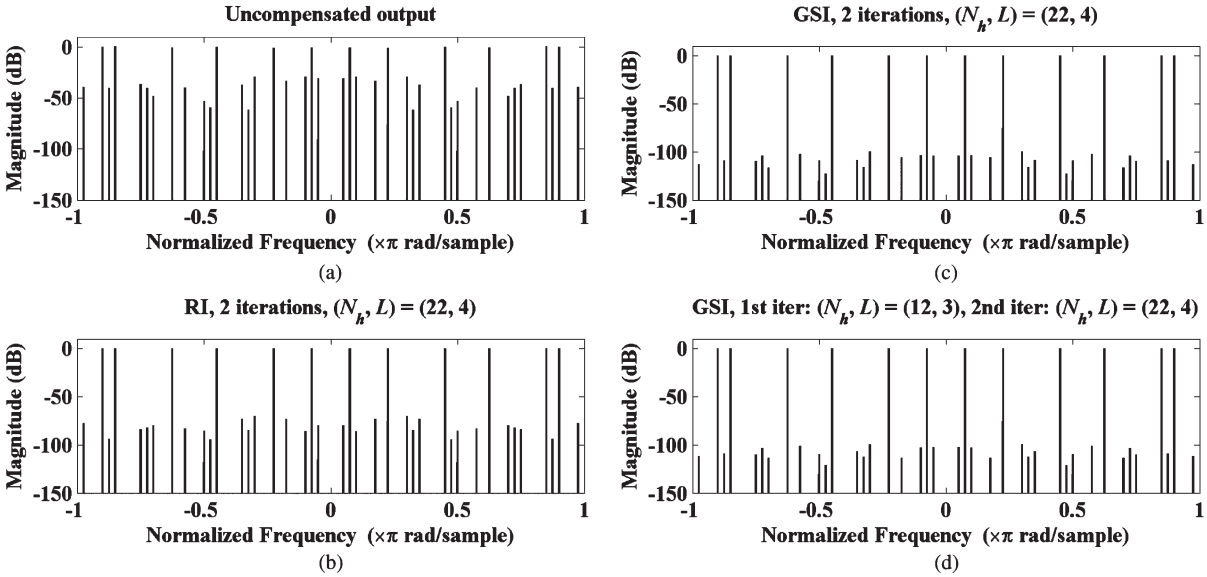

Fig. 6. (a) Uncompensated output spectrum. (b) Output spectrum obtained using the RI after two iterations. (c) Output spectrum obtained using the GSI after two iterations. (d) Output spectrum obtained using the GSI after two iterations, and a VDF of lower filter order and fewer subfilters are used in the first iteration.

the second system. Finally, we obtain the lower bound of SNDR after (K_1, K_2) iterations as

$$SNDR^{(K_1,K_2)} \geq \frac{M}{\sum_{n=0}^{M-1} \int_{-\alpha\pi}^{\alpha\pi} \left| P_n + G_{n,1}^{K_1} Q_{n,1} + G_{n,2}^{K_2} Q_{n,2} \right|^2 d\omega}. \quad (40)$$

Again, for sufficiently large K_1 and K_2, we notice that the ultimate SNDR is eventually governed by P_n, which depends solely on the filter approximation errors for the two time-varying systems.

VII. Design Examples

A. Example 1: Compensation of Bandwidth Mismatch

In this section, we shall investigate the performance of the proposed iterative structure by means of computer simulations. For comparison purpose, we shall also consider the promising compensation structure proposed in [21]. As we mentioned in Section III, this structure can be regarded as the RI.

We shall consider bandwidth mismatches in an M-channel TI ADC. The corresponding channel frequency response is given by

$$F_n(j\Omega) = \frac{1}{1 + j\frac{\Omega}{\Omega_n^c}} \frac{1 - e^{-(\Omega_n^c T + j\Omega T)}}{1 - e^{-(\Omega_n^c T + jM\Omega T)}} \quad (41)$$

where Ω_n^c is a time-varying cutoff frequency. Interested readers are referred to [21] and [24] for more details of this model. We assumed that the parameters Ω_n^c have been estimated and the desired frequency response is chosen as

$$\overline{F}(j\Omega) = \frac{1}{1 + j\frac{\Omega}{\pi/T}} \quad (42)$$

which approximates the average response of $F_n(e^{j\omega})$ as discussed in Section V. According to the DT model of TI ADC in Fig. 2, we express the ideal frequency response $D_n(e^{j\omega})$ as

$$D_n(e^{j\omega}) = \frac{F_n(e^{j\omega})}{\overline{F}(e^{j\omega})} = \frac{1 + j\frac{\omega}{\pi}}{1 + j\frac{\omega}{(1+\phi_n)\pi}} \frac{1 - e^{-[(1+\phi_n)\pi + j\omega]}}{1 - e^{-[(1+\phi_n)\pi + jM\omega]}} \quad (43)$$

where $\phi_n = \Omega_n^c T/\pi - 1$. We can see that the response $D_n(e^{j\omega})$ varies with a single spectral parameter ϕ_n, and therefore, it can be expressed as a function of frequency and spectral parameter, i.e., $D(e^{j\omega}, \phi_n) = D_n(e^{j\omega})$. As discussed in Section IV, we employ a VDF $H(e^{j\omega}, \phi)$ in the form of (14) to approximate $D(e^{j\omega}, \phi)$ by solving the following minimax problem:

$$\min \max_{(\omega,\alpha)\in\Psi} \left| H(e^{j\omega}, \phi) - D(e^{j\omega}, \phi) \right| \quad (44)$$

where Ψ collectively denotes the frequency and tuning range of interest. Once it is solved, we obtain the VDF subfilter coefficients $c_l[n_0]$ in (13) and establish the linear model in (4) with $h_n[n_0] = h[n_0, \phi_n]$. Using this model, we can iteratively find $x[n]$ given $y[n]$. In the simulation hereinafter, we consider a five-channel TI ADC (i.e., $M = 5$). Also, we choose $\Omega_n^c = [1, 0.94, 1.1, -1.1, 1.04]\pi/T$, and hence, the spectral parameter of $D(e^{j\omega}, \phi_n)$ is given by $\phi_n = [0, -0.06, 0.1, -0.1, 0.04]$. As an illustration, we assume that $x[n] = \sum_{k=1}^{6} \cos(n\omega_k)$ with $[\omega_1, \ldots, \omega_6] = [0.075, 0.225, 0.45, 0.625, 0.85, 0.9]\pi$. Fig. 6(a) shows the uncorrected output spectrum, i.e., the spectrum of $y[n]$. It can be seen that the largest aliasing component is about -29 dB.

According to the maximum input frequency and ϕ_n defined earlier, Ψ in (44) is chosen as $\omega \in [-0.9\pi, 0.9\pi]$ and $\phi \in [-0.1, 0.1]$. A VDF is designed using the method in [36] with the following specifications: $N_{h1} = N_{h2} = N_h = 22$ and the number of subfilters $L = 4$. Given the VDF so obtained, the cost function λ in (16) is 0.82, which implies that the sufficient

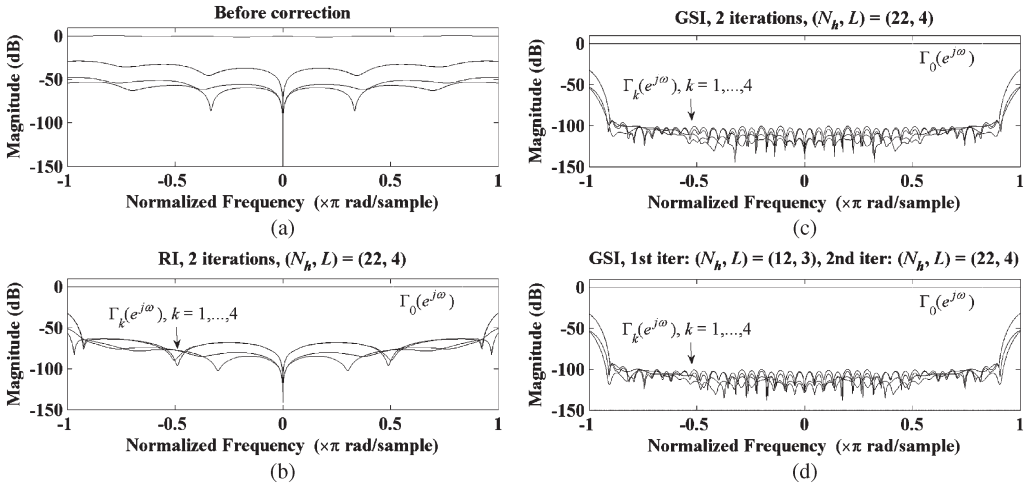

Fig. 7. (a)–(d) System responses $\Gamma_k^{(m)}(e^{j\omega})$, $k = 0, 1 \ldots, 4$, for the output spectra shown in Fig. 6(a)–(d), respectively. The superscript (m) of $\Gamma_k^{(m)}(e^{j\omega})$ is dropped in the figures for notation simplicity.

condition is satisfied. Fig. 6(b) and (c) shows, respectively, the compensated spectra obtained using the RI (i.e., the structure in [21]) and the GSI after two iterations. It can be seen that the largest spurs are reduced to -70.21 and -99.83 dB for the RI and GSI, respectively. This suggests the superiority of the GSI over the RI for a comparable implementation complexity.

Up to now, the VDFs used in all iterations are assumed to be identical, which is merely a particular configuration of our general iterative framework. In fact, it is possible to use VDFs with lower filter order and/or fewer subfilters in the first few iterations, so as to further reduce the overall implementation complexity. We notice that similar observation was considered in [21]. Here, we have extended this idea to various iterative methods, including the GSI, in a more general framework considered in this paper. Fig. 4(d) shows the compensated spectrum obtained using the GSI with two different VDFs, for which the VDF parameters used in the first iteration are $(N_h, L) = (12, 3)$ and those in the second iteration are kept as $(N_h, L) = (22, 4)$. It can be seen that such configuration has similar performance as compared with the result in Fig. 6(c) while offering lower implementation complexity.

Using the results in (22) and (23), Fig. 7(a)–(d) shows the equivalent system frequency responses, $\Gamma_k^{(m+1)}(e^{j\omega})$, which produce the output spectra shown in Fig. 6(a)–(d), respectively. As expected, the reduction of the largest aliasing component is in line with the maximum attenuation due to $\Gamma_k^{(m+1)}(e^{j\omega})$.

B. Example 2: Study of the SNDR Performance

In this example, we study how the SNDR is improved as the number of iterations increases. The reconstruction performance is assessed using the SNDR as defined in (26). For simplicity, we consider the same TI ADC settings as in Example 1, except that $x[n]$ is obtained from a white noise sequence band-limited in the frequency region $\omega \in [-0.9\pi, 0.9\pi]$. Fig. 8 shows the SNDR performances of the RI and GSI algorithms. As expected, the SNDRs of these two algorithms improve with the number of iterations. Also, it can be seen that the GSI and RI converge in nearly two and four iterations, respectively.

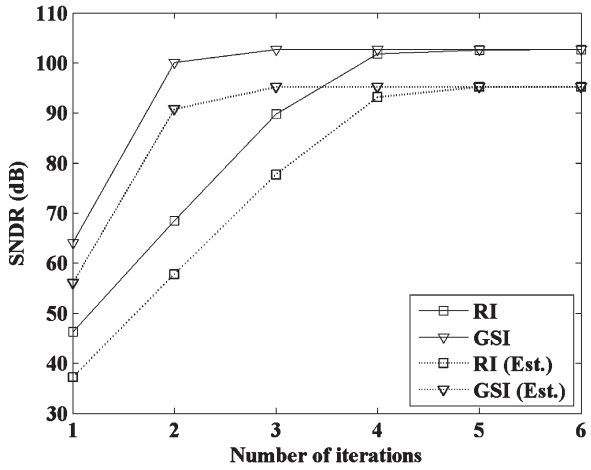

Fig. 8. Performances of the GSI and RI (i.e., conventional structure in [19]) for a band-limited white noise sequence. The dotted lines represent the estimated (Est.) SNDR lower bounds of the GSI and GI.

Note that both algorithms offer the same ultimate SNDRs upon convergence, which are mainly restricted by the filter approximation error, as discussed in Section V-C.

To further verify the theoretical results presented earlier, the lower bound of the SNDR derived in (27) is also plotted as dotted lines in Fig. 8. It can be seen that the performance of both RI and GSI can be well predicted by the theoretical lower bound. Therefore, it is useful to practical designers to predict and evaluate the final SNDR performance and the minimum number of iterations required by the iterative algorithms under the general framework in (6).

Next, we study the effect of filter approximation error on the SNDR performance. In VDF design problem, it is well known that the filter approximation error is mainly determined by subfilter length, subfilter number, and frequency and tuning range of interest [36]. More precisely, the SNDR will improve with the following: 1) increased filter length; 2) increased number of subfilters; 3) reduced passband width; and 4) reduced tuning range of the VDF. While the latter two depend on the ADC specifications at hand, we can freely choose the subfilter length and number to achieve arbitrary SNDR. Due to page

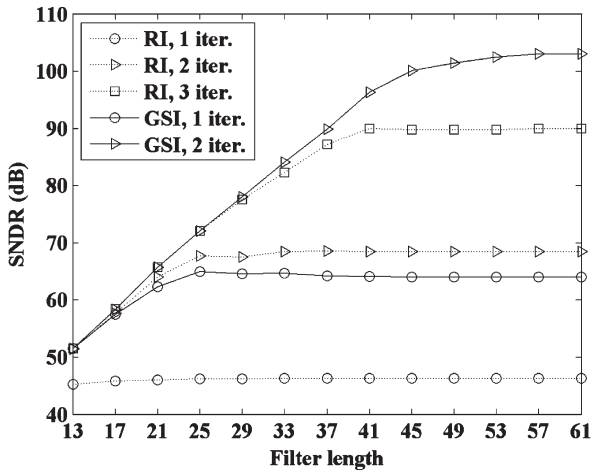

Fig. 9. Performance comparison (SNDR versus filter length) of the GSI and RI with different number of iterations (iter.).

limitation, we only focus on the effect of subfilter length. In particular, we consider the set of subfilter lengths given by $P = 13, 17, \ldots, 61$. Fig. 9 shows the SNDR performance of the RI and GSI with different numbers of iterations versus the filter length. It can be seen that the GSI outperforms the RI in the sense that the former generally needs fewer iterations to achieve higher SNDR. Moreover, it is worth noting that all the SNDR curves exhibit similar characteristics. At the beginning, the SNDR for a given number of iterations increases linearly because the filter approximation error decreases as the filter length increases. In this region, if the iterative algorithm converges, then it reaches the ultimate SNDR which mainly depends on the filter approximation error. This fact can be observed in the SNDR curves of the third RI and the second GSI when the subfilter length is less than 29. When the subfilter length is further increased, the SNDR curves eventually level off because, in this region, the corresponding SNDR is mainly governed by the convergence rate of the iterative methods, i.e., $G_n(e^{j\omega})$ in (27). From the aforementioned results, it is clear that the GSI converges much faster than the RI. In other words, the GSI can achieve a given SNDR specification with fewer iterations and, hence, lower implementation complexity than the RI, particularly if the system is pipelined.

C. Example 3: Compensation of Multiple Mismatches

In this example, we study the effectiveness of the proposed algorithm in Section VI when it is applied to multiple time-varying systems. As an illustration, we consider the following channel frequency response:

$$F_n(j\Omega) = \frac{1}{1 + j\frac{\Omega}{\Omega_n^c}} \frac{1 - e^{-(\Omega_n^c T + j\Omega T)}}{1 - e^{-(\Omega_n^c T + jM\Omega T)}} e^{-j\Omega T\alpha_n}$$
$$= F_{n,1}(j\Omega) F_{n,2}(j\Omega) \tag{45}$$

where $F_{n,1}(j\Omega)$ is defined similarly as the bandwidth mismatch in (41) and $F_{n,2}(j\Omega) = e^{-j\Omega T\alpha_n}$ corresponds to the timing mismatch. We assume that the bandwidth mismatch characteristic is identical to that in Example 1 for a five-channel TI ADC, and therefore, we can directly apply the VDF designed in Example 1 for the correction of this mismatch. For the second system, we assume that the five subconverters exhibit time offsets $-\alpha_n T$, $n = 0, 1, 2, 3, 4$, with respect to the ideal sampling time $t = nT$, where $\alpha_n = [0, 0.01, -0.05, -0.01, 0.05]$. Here, we simply choose $\overline{F}_2(e^{j\omega}) = 1$ so that the ideal frequency response is given by

$$D_{n,2}(e^{j\omega}) = D_2(e^{j\omega}, \alpha_n) = e^{-j\omega\alpha_n} \tag{46}$$

where $D_2(e^{j\omega}, \alpha) = e^{-j\omega\alpha}$ is the corresponding desired DT frequency response of the VDF with spectral parameter α. In the literature, it is sometimes referred to as variable fractional delay digital filter (VFDDF), which finds important application of sampling rate conversion in software radio receivers [31] and timing mismatch correction in TI ADCs [16]–[18]. The parameters of the VDF (or VFDDF) used for the iterative correction of the timing mismatch are summarized as follows: $\omega \in [-0.9\pi, 0.9\pi]$, $\alpha \in [-0.05, 0.05]$, $N_{h1} = N_{h2} = N_h = 23$, and $L = 4$.

Fig. 10(a) shows the uncorrected signal spectrum which is obtained by applying both types of mismatches to the multicosine signal considered in Example 1. As already demonstrated in Example 1, we first apply the GSI two times to this uncorrected signal, resulting in the spectrum shown in Fig. 10(b). It can be seen that the aliasing components still exist in the spectrum, which is caused by the timing mismatch. Then, we employ the VFDDF designed earlier to iteratively correct the timing mismatch. Fig. 10(c) and (d) shows the spectra after applying the GSI one and two times, respectively. It can be seen that the aliasing components are suppressed as the number of iterations increases and the desired signal up to an accuracy of nearly 100 dB is successfully recovered in Fig. 10(d) after $(K_1, K_2) = (2, 2)$ iterations.

VIII. Conclusion

A new iterative framework for the correction of frequency response mismatches in TI ADCs has been presented. It encumbrances the conventional RI and other efficient iterative correction algorithms such as the GSI and simplifies their design, implementation, and performance analysis. The efficient GSI is studied in detail, and a Farrow-based VDF structure is developed for its implementation, which requires few general-purpose multipliers. Important advantages of the proposed iterative structure are the following: 1) The implementation complexity is independent of the number of channels, and only a few iterations are required for convergence; and 2) the use of VDFs enables the online adaptation of the possibly changing channel mismatch errors with low complexity. Also, the convergence and performance are analyzed. These results are useful to the performance prediction, design, and evaluation of such TI ADCs to meet different design specifications. Moreover, the proposed iterative structure is extended to cope with systems involving more than one type of mismatches using a cascading approach. Simulation results further showed that the proposed method has better performance than conventional structures using RI.

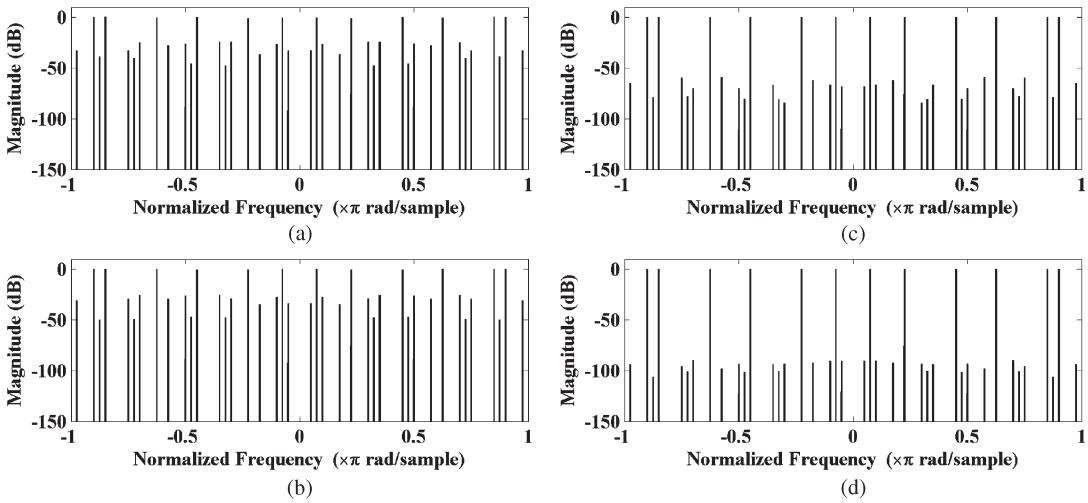

Fig. 10. (a) Uncompensated output spectrum in two cascaded time-varying systems, one is for bandwidth mismatch and the other is for timing mismatch. Output spectrum obtained using the GSI after (b) (2,0) iterations, (c) (2,1) iterations, and (d) (2,2) iterations. (K_1, K_2) indicates that the output signal is obtained by first applying K_1 iterations to solve the first system and then K_2 iterations to solve the second system.

Finally, this paper is concluded by pointing out two possible ways of extending the proposed approach. The first one is its possible application to online calibration of TI ADCs, which involves the process of simultaneously estimating and compensating for the channel mismatches [7], [8], [13], [14], [38]. For instance, in [38], a reference signal, which is provided by an extra low-resolution ADC, is employed to estimate the coefficients of the time-varying compensation filter by means of least mean square algorithm. In this paper, we consider only the compensation part where the channel models are assumed to be known or accurately estimated. On the other hand, it is possible to utilize the proposed compensation structure as a part of calibration process. We expect that the proposed compensation structure enables efficient online calibration with few adaptation parameters because most of its multipliers are fixed. To do so, appropriate measure is needed to relate the estimation error with the spectral parameters in the proposed structure, and it is minimized for the adaptive update of the spectral parameters.

Another possible direction is to incorporate the prior knowledge of input signal in the design procedure, so as to further improve the performance of the proposed approach. It was shown in [42] that realistic knowledge of input signal would lead to reduced implementation complexity in the conventional filter bank compensation structure. For the proposed approach, we need to include this extra knowledge in the performance measures, such as system spectrum, SFDR, and SNDR, for the design of VDFs.

Appendix A
Sufficient Condition for Convergence of the GSI

According to [40, Th. 5.11], it can be shown that the worst case error in (9) for the GSI satisfies

$$\left\|\boldsymbol{e}^{(m+1)}\right\|_\infty \left(1-\sum_{n_0>0}\frac{|h_n[n_0]|}{|h_n[0]|}\right) \le \left\|\boldsymbol{e}^{(m)}\right\|_\infty \sum_{n_0<0}\frac{|h_n[n_0]|}{|h_n[0]|} \tag{A1}$$

where $\boldsymbol{e}^{(m)} = \boldsymbol{x} - \boldsymbol{x}^{(m)}$ and $\|\boldsymbol{e}^{(m)}\|_\infty = \max_n |e^{(m)}[n]|$. Therefore, if $\boldsymbol{A}$ is a strictly diagonal dominant matrix, i.e., $|h_n[0]| > \sum_{n_0<0}|h_n[n_0]| + \sum_{n_0>0}|h_n[n_0]|$, then we have

$$0 < \sum_{n_0<0}\frac{|h_n[n_0]|}{|h_n[0]|} < 1 - \sum_{n_0>0}\frac{|h_n[n_0]|}{|h_n[0]|}. \tag{A2}$$

This implies that $\|\boldsymbol{e}^{(m+1)}\|_\infty < \|\boldsymbol{e}^{(m)}\|_\infty < \cdots < \|\boldsymbol{e}^{(0)}\|_\infty$, and hence, the GSI is convergent.

Appendix B
Comparison of the GSI and RI

Similar to (A1), it can be shown that the worst case error of the RI in (7) is given by

$$\left\|\boldsymbol{e}^{(m+1)}\right\|_\infty \le \left\|\boldsymbol{e}^{(m)}\right\|_\infty \left(|1-|h_n[0]|| + \sum_{n_0<0}|h_n[n_0]| + \sum_{n_0>0}|h_n[n_0]|\right). \tag{A3}$$

Defining $\theta_{n,L} = \sum_{n_0<0}|h_n[n_0]|$, $\theta_{n,R} = \sum_{n_0>0}|h_n[n_0]|$, $\gamma_n^{\mathrm{RI}} = |1-|h_n[0]|| + \theta_{n,L} + \theta_{n,R}$, and $\gamma_n^{\mathrm{GSI}} = \theta_{n,L}/(|h_n[0]| - \theta_{n,R})$ derived in (A1), we want to prove that $\gamma_n^{\mathrm{GSI}} < \gamma_n^{\mathrm{RI}}$ if $\boldsymbol{A}$ is a strictly diagonal dominant matrix, i.e., $|h_n[0]| > \theta_{n,L} + \theta_{n,R}$.

Given $|h_n[0]| > \theta_{n,L} + \theta_{n,R}$, it is easy to show that

$$\gamma_n^{\mathrm{GSI}} < \gamma_n = \frac{\theta_{n,L}+\theta_{n,R}}{|h_n[0]|}. \tag{A4}$$

Also, it can be seen that the more dominant the diagonal of $\boldsymbol{A}$ (i.e., $|h_n[0]|$), the more rapid the convergence should be. Now, consider

$$\gamma_n^{\mathrm{RI}} - \gamma_n = \frac{|1-h_n[0]|\,|h_n[0]| + (|h_n[0]|-1)\,(\theta_{n,L}+\theta_{n,R})}{|h_n[0]|}. \tag{A5}$$

Using the inequality $|h_n[0]| > \theta_{n,L} + \theta_{n,R}$ again, we have

$$\gamma_n^{\mathrm{RI}} - \gamma_n > \frac{(|1 - h_n[0]| + |h_n[0]| - 1)\,(\theta_{n,L} + \theta_{n,R})}{|h_n[0]|}. \tag{A6}$$

Since $|1 - h_n[0]| + |h_n[0]| - 1 \geq 0$ for all $h_n[0]$, we finally obtain

$$\gamma_n^{\mathrm{GSI}} < \gamma_n < \gamma_n^{RI}. \tag{A7}$$

This suggests that the GSI should usually converge faster than the RI if $\boldsymbol{A}$ is a strictly diagonal dominant matrix.

Appendix C
Derivation of the Lower Bound of the SNDR

First of all, we want to derive an expression for $R_n^{(m+1)}(e^{j\omega}) = X(e^{j\omega}) - X_n^{(m+1)}(e^{j\omega})$ in terms of $X(e^{j\omega})$ for the denominator of (26) at time instant n. To investigate the effect of practical filters, we further rewrite $R_n^{(m+1)}(e^{j\omega})$ as follows:

$$R_n^{(m+1)}(e^{j\omega}) = \left[X(e^{j\omega}) - \hat{X}_n(e^{j\omega})\right] + \left[\hat{X}_n(e^{j\omega}) - X_n^{(m+1)}(e^{j\omega})\right] \tag{A8}$$

where the term in the first square bracket represents the error due to filter approximation and the second one represents the error in the $(m+1)$th iteration. Because of (11b) and (17), $\hat{X}_n(e^{j\omega})$ also satisfies

$$B_n(e^{j\omega})\hat{X}_n(e^{j\omega}) = C_n(e^{j\omega})\hat{X}_n(e^{j\omega}) + Y_n(e^{j\omega}). \tag{A9}$$

Subtracting (11a) from (A9) yields

$$\begin{aligned}\hat{X}_n(e^{j\omega}) - X_n^{(m+1)}(e^{j\omega}) &= G_n(e^{j\omega})\left[\hat{X}_n(e^{j\omega}) - X_n^{(m)}(e^{j\omega})\right] \\ &\vdots \\ &= G_n^{m+1}(e^{j\omega})\left[\hat{X}_n(e^{j\omega}) - X_n^{(0)}(e^{j\omega})\right].\end{aligned} \tag{A10}$$

Consequently, with (17)–(19) and (A10), (A8) can be expressed as

$$R_n^{(m+1)}(e^{j\omega}) = \left[P_n(e^{j\omega}) + G_n^{m+1}(e^{j\omega})Q_n(e^{j\omega})\right] X(e^{j\omega}) \tag{A11}$$

where $P_n(e^{j\omega}) = 1 - D_n(e^{j\omega})H_n^{-1}(e^{j\omega})$ and $Q_n(e^{j\omega}) = D_n(e^{j\omega})[H_n^{-1}(e^{j\omega}) - 1]$. Using again the bifrequency mapping as in (22), we have

$$R^{(m+1)}(e^{j\omega}) = \sum_{k=0}^{M-1} \tilde{V}_k^{(m+1)}\left(e^{j\omega}W_M^k\right) X\left(e^{j\omega}W_M^k\right) \tag{A12}$$

where $\tilde{V}_k^{(m+1)}(e^{j\omega}) = (1/M)\sum_{n=0}^{M-1} V_n^{(m+1)}(e^{j\omega})W_M^{nk}$ and $V_n^{(m+1)}(e^{j\omega}) = P_n(e^{j\omega}) + G_n^{m+1}(e^{j\omega})Q_n(e^{j\omega})$. Substituting (A11) into the denominator of (26) gives

$$\begin{aligned}&\int_{-\pi}^{\pi} \left|R^{(m+1)}(e^{j\omega})\right|^2 d\omega \\ &\quad\leq \frac{1}{M^2}\sum_{k=0}^{M-1}\sum_{n=0}^{M-1}\int_{-\pi}^{\pi}\left|V_n^{(m+1)}\left(e^{j\omega}W_M^k\right)X\left(e^{j\omega}W_M^k\right)\right|^2 d\omega \\ &\quad= \frac{1}{M}\sum_{n=0}^{M-1}\int_{-\alpha\pi}^{\alpha\pi}\left|V_n^{(m+1)}(e^{j\omega})X(e^{j\omega})\right|^2 d\omega \\ &\quad\leq \frac{1}{M}\int_{-\alpha\pi}^{\alpha\pi}\left|X(e^{j\omega})\right|^2 d\omega \sum_{n=0}^{M-1}\int_{-\alpha\pi}^{\alpha\pi}\left|V_n^{(m+1)}(e^{j\omega})\right|^2 d\omega.\end{aligned} \tag{A13}$$

Note that the second equality in (A13) is derived from the fact that

$$\begin{aligned}&\int_{-\pi}^{\pi}\left|V_n^{(m)}\left(e^{j\omega}W_M^k\right)\cdot X\left(e^{j\omega}W_M^k\right)\right|^2 d\omega \\ &\quad= \int_{-\pi}^{\pi}\left|V_n^{(m)}(e^{j\omega})\cdot X(e^{j\omega})\right|^2 d\omega \\ &\quad= \int_{-\alpha\pi}^{\alpha\pi}\left|V_n^{(m)}(e^{j\omega})\cdot X(e^{j\omega})\right|^2 d\omega\end{aligned}$$

for $k = 0, 1, \ldots, M-1$. Substituting (A13) into (26), we obtain the desired lower bound of SNDR after $(m+1)$ iterations as (27)

$$\begin{aligned}&SNDR^{(m+1)} \\ &\quad\geq \frac{M}{\sum_{n=0}^{M-1}\int_{-\alpha\pi}^{\alpha\pi}\left|V_n^{(m+1)}(e^{j\omega})\right|^2 d\omega} \\ &\quad= \frac{M}{\sum_{n=0}^{M-1}\int_{-\alpha\pi}^{\alpha\pi}\left|P_n(e^{j\omega}) + G_n^{m+1}(e^{j\omega})Q_n(e^{j\omega})\right|^2 d\omega}.\end{aligned} \tag{A14}$$

References

[1] P. Burns, *Software Defined Radio for 3G*. Norwood, MA: Artech House, 2002.

[2] R. H. Walden, "Analog-to-digital converter survey and analysis," *IEEE J. Sel. Areas Commun.*, vol. 17, no. 4, pp. 539–550, Apr. 1999.

[3] W. C. Black and D. A. Hodges, "Time interleaved converter arrays," *IEEE J. Solid-State Circuits*, vol. SSC-15, no. 6, pp. 1022–1029, Dec. 1980.

[4] A. Petraglia and S. K. Mitra, "Analysis of mismatch effects among A/D converters in a time-interleaved waveform digitizer," *IEEE Trans. Instrum. Meas.*, vol. 40, no. 5, pp. 831–835, Oct. 1991.

[5] C. Vogel, "The impact of combined channel mismatch effects in time-interleaved ADCs," *IEEE Trans. Instrum. Meas.*, vol. 54, no. 1, pp. 415–427, Feb. 2005.

[6] Y. C. Jenq, "Perfect reconstruction of digital spectrum from nonuniformly sampled signals," *IEEE Trans. Instrum. Meas.*, vol. 46, no. 3, pp. 649–652, Jun. 1997.

[7] H. Jin and E. K. F. Lee, "A digital-background calibration technique for minimizing timing-error effects in time-interleaved ADCs," *IEEE Trans. Circuits Syst. II, Analog Digit. Signal Process.*, vol. 47, no. 7, pp. 603–613, Jul. 2000.

[8] C. Y. Wang and J. T. Wu, "A background timing-skew calibration technique for time-interleaved analog-to-digital converters," *IEEE Trans. Circuits Syst. II, Exp. Briefs*, vol. 53, no. 4, pp. 299–303, Apr. 2006.

[9] J. M. D. Pereira, P. M. B. S. Girao, and A. M. C. Serra, "An FFT-based method to evaluate and compensate gain and offset errors of interleaved ADC systems," *IEEE Trans. Instrum. Meas.*, vol. 53, no. 2, pp. 423–430, Apr. 2004.
[10] R. S. Prendergast, B. C. Levy, and P. J. Hurst, "Reconstruction of bandlimited periodic nonuniformly sampled signals through multirate filter banks," *IEEE Trans. Circuits Syst. I, Reg. Papers*, vol. 51, no. 8, pp. 1612–1622, Aug. 2004.
[11] H. Johansson and P. Löwenborg, "Reconstruction of nonuniformly sampled bandlimited signals by means of time-varying discrete-time FIR filters," *EURASIP J. Appl. Signal Process.*, vol. 2006, pp. 1–18, 2006, Article ID 64185.
[12] Y. C. Eldar and A. V. Oppenheim, "Filterbank reconstruction of bandlimited signals from nonuniform and generalized samples," *IEEE Trans. Signal Process.*, vol. 48, no. 10, pp. 2864–2875, Oct. 2000.
[13] S. Huang and B. C. Levy, "Adaptive blind calibration of timing offset and gain mismatch for two-channel time-interleaved ADCs," *IEEE Trans. Circuits Syst. I, Reg. Papers*, vol. 53, no. 6, pp. 1278–1288, Jun. 2006.
[14] S. Huang and B. C. Levy, "Blind calibration of timing offset for four-channel time-interleaved ADCs," *IEEE Trans. Circuits Syst. I, Reg. Papers*, vol. 54, no. 4, pp. 863–876, Apr. 2006.
[15] Y. X. Zou, S. L. Zhang, Y. C. Lim, and X. Chen, "Timing mismatch compensation in time-interleaved ADCs based on multichannel Lagrange polynomial interpolation," *IEEE Trans. Instrum. Meas.*, vol. 60, no. 4, pp. 1123–1131, Apr. 2011.
[16] J. Selva, "Functionally weighted Lagrange interpolation of band-limited signals from nonuniform samples," *IEEE Trans. Signal Process.*, vol. 57, no. 1, pp. 168–181, Jan. 2009.
[17] Y. C. Lim, Y. X. Zou, J. W. Lee, and S. C. Chan, "Time-interleaved analog-to-digital-converter compensation using multichannel filters," *IEEE Trans. Circuits Syst. I, Reg. Papers*, vol. 56, no. 10, pp. 2234–2347, Oct. 2009.
[18] S. Tertinek and C. Vogel, "Reconstruction of nonuniformly sampled bandlimited signals using a differentiator-multiplier cascade," *IEEE Trans. Circuits Syst. I, Reg. Papers*, vol. 55, no. 8, pp. 2273–2286, Sep. 2008.
[19] K. M. Tsui and S. C. Chan, "A versatile iterative framework for the reconstruction of bandlimited signals from their nonuniform samples," *J. Signal Process. Syst.*, vol. 62, no. 3, pp. 459–468, Mar. 2011.
[20] K. M. Tsui, "Efficient design and realization of digital IFs and time-interleaved analog-to-digital converters for software radio receivers," Ph.D. dissertation, Univ. Hong Kong, Hong Kong, Jul., 2008.
[21] C. Vogel and S. Mendel, "A flexible and scalable structure to compensate frequency response mismatches in time-interleaved ADCs," *IEEE Trans. Circuits Syst. I, Reg. Papers*, vol. 56, no. 11, pp. 2463–2475, Nov. 2009.
[22] H. Johansson, "A polynomial-based time-varying filter structure for the compensation of frequency-response mismatch errors in time-interleaved ADCs," *IEEE J. Sel. Topics Signal Process.*, vol. 3, no. 3, pp. 384–396, Jun. 2009.
[23] M. Seo, M. Rodwell, and U. Madhow, "Comprehensive digital correction of mismatch errors for a 400-Msamples/s 80-dB SFDR time-interleaved analog-to-digital converter," *IEEE Trans. Microw. Theory Tech.*, vol. 53, no. 3, pp. 1072–1082, Apr. 2005.
[24] T. H. Tsai, P. J. Hurst, and S. H. Lewis, "Bandwidth mismatch and its correction in time-interleaved analog-to-digital converters," *IEEE Trans. Circuits Syst. II, Exp. Briefs*, vol. 53, no. 10, pp. 1133–1137, Oct. 2006.
[25] P. Satarzadeh, B. Levy, and P. Hurst, "Bandwidth mismatch correction for a two-channel time-interleaved A/D converter," in *Proc. IEEE ISCAS*, May 2007, pp. 1705–1708.
[26] C. K. S. Pun, S. C. Chan, K. S. Yeung, and K. L. Ho, "On the design and implementation of FIR and IIR digital filters with variable frequency characteristics," *IEEE Trans. Circuits Syst. II, Analog Digit. Signal Process.*, vol. 49, no. 11, pp. 689–703, Nov. 2002.
[27] C. W. Farrow, "A continuously variable digital delay element," in *Proc. IEEE ISCAS*, 1988, vol. 3, pp. 2641–2645.
[28] S. C. Chan, K. M. Tsui, K. S. Yeung, and T. I. Yuk, "Design and complexity optimization of a new digital IF for software radio receivers with prescribed output accuracy," *IEEE Trans. Circuits Syst. I, Reg. Papers*, vol. 54, no. 2, pp. 351–366, Feb. 2007.
[29] Y. Saad, *Iterative Methods for Sparse Linear Systems*. Boston, MA: PWS, 1996.
[30] C. Loeffler and C. Burrus, "Optimal design of periodically time-varying and multirate digital filters," *IEEE Trans. Acoust., Speech, Signal Process.*, vol. ASSP-32, no. 5, pp. 991–997, Oct. 1984.
[31] J. S. Prater and C. M. Loeffler, "Analysis and design of periodically time-varying IIR filters, with applications to transmultiplexing," *IEEE Trans. Signal Process.*, vol. 40, no. 11, pp. 2715–2725, Nov. 1992.
[32] Y. C. Jenq, "Digital spectra of nonuniformly sampled signals: A robust sampling time offset estimation algorithm for ultra high speed waveform digitizers using interleaving," *IEEE Trans. Instrum. Meas.*, vol. 39, no. 1, pp. 71–75, Feb. 1990.
[33] Z. Feng, H. He, and R. Unbehauen, "The determination of the generalized frequency response for linear periodically shift-variant digital filters," in *Proc. IEEE MWSCAS*, Nov. 1992, vol. 1, pp. 591–593.
[34] P. P. Vaidyanathan, *Multirate Systems and Filter Banks*. Englewood Cliffs, NJ: Prentice-Hall, 1993.
[35] R. Ishii and M. Kakishita, "Analysis of a periodically time-varying digital filter," in *Proc. IEEE ICASSP*, 1986, vol. 11, pp. 2607–2610.
[36] K. M. Tsui, S. C. Chan, and K. W. Tse, "Design of complex-valued variable digital filters and its application to the realization of arbitrary sampling rate conversions for complex signals," *IEEE Trans. Circuits Syst. II, Exp. Briefs*, vol. 52, no. 7, pp. 424–428, Jul. 2005.
[37] K. M. Tsui and S. C. Chan, "Iterative correction of frequency response mismatches in time-interleaved ADCs: A novel framework and case study in OFDM systems," in *Proc. IEEE ICGCS*, Jun. 2010, pp. 253–258.
[38] S. Saleem and C. Vogel, "Adaptive compensation of frequency response mismatches in high-resolution time-interleaved ADCs using a low-resolution ADC and a time-varying filter," in *Proc. IEEE ISCAS*, 2010, pp. 561–564.
[39] S. Ponnuru and U. Madhow, "Scalable mismatch compensation for time-interleaved A/D converters in OFDM reception," in *Proc. IEEE WCNC*, Apr. 2010, pp. 1–6.
[40] G. Meurant, *Computer Solutions of Large Linear Systems*. Amsterdam, The Netherlands: Elsevier, 1999.
[41] H. Johansson and P. Löwenborg, "A least-squares filter design technique for the compensation of frequency-response mismatch errors in time interleaved A/D converters," *IEEE Trans. Circuits Syst. II, Exp. Briefs*, vol. 55, no. 11, pp. 1154–1158, Nov. 2008.
[42] D. Marelli, K. Mahata, and M. Fu, "Linear LMS compensation for timing mismatch in time-interleaved ADCs," *IEEE Trans. Circuits Syst. I, Reg. Papers*, vol. 56, no. 11, pp. 2476–2486, Nov. 2009.
[43] K. S. Yeo and K. Roy, *Low Voltage, Low Power VLSI Subsystems*. New York: McGraw-Hill, 2005.

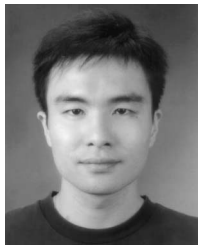

K. M. Tsui received the B.Eng., M.Phil., and Ph.D. degrees in electrical and electronic engineering from The University of Hong Kong, Pokfulam, Hong Kong, in 2001, 2004, and 2008, respectively.

He is currently a Postdoctoral Fellow with the Department of Electrical and Electronic Engineering, The University of Hong Kong. His main research interests are in array signal processing, high-speed A-D converter architecture, biomedical signal processing, digital signal processing, multirate filter bank and wavelet design, and digital filter design, realization, and application.

S. C. Chan (S'87–M'92) received the B.Sc. (Eng.) and Ph.D. degrees from The University of Hong Kong, Pokfulam, Hong Kong, in 1986 and 1992, respectively.

He was with the City Polytechnic of Hong Kong, Kowloon, Hong Kong, in 1990 as an Assistant Lecturer and later as a University Lecturer. Since 1994, he has been with the Department of Electrical and Electronic Engineering, The University of Hong Kong, and is currently a Professor. He was a Visiting Researcher at Microsoft Corporation, Redmond, WA; Microsoft Corporation, Beijing, China; University of Texas, Arlington; and Nanyang Technological University, Singapore. His research interests include fast transform algorithms, filter design and realization, multirate and biomedical signal processing, communications and array signal processing, high-speed A-D converter architecture, bioinformatics, and image-based rendering.

Dr. Chan is currently a member of the Digital Signal Processing Technical Committee of the IEEE Circuits and Systems Society and an Associate Editor of the *Journal of Signal Processing Systems*. He was the Chairman of the IEEE Hong Kong Chapter of Signal Processing 2000–2002 and an organizing committee member of the IEEE International Conference on Acoustics, Speech, and Signal Processing 2003 and the International Conference on Image Processing 2010, and an Associate Editor of the IEEE TRANSACTIONS ON CIRCUITS AND SYSTEMS—I.